Journal of Hydrology 510 (2014) 393–402

Contents lists available at ScienceDirect

Journal of Hydrology

journal homepage: www.elsevier.com/locate/jhydrol

Assessing the effect of different river water level interpolation schemes on modeled groundwater residence times

Samuel Diem [a,b,*], Philippe Renard [b], Mario Schirmer [a,b]

[a] Eawag, Swiss Federal Institute of Aquatic Science and Technology, Water Resources & Drinking Water, Überlandstrasse 133, 8600 Dübendorf, Switzerland
[b] University of Neuchâtel, Centre for Hydrogeology and Geothermics, Rue Emile-Argand 11, 2000 Neuchâtel, Switzerland

ARTICLE INFO

Article history:
Received 22 July 2013
Received in revised form 21 December 2013
Accepted 28 December 2013
Available online 8 January 2014
This manuscript was handled by Corrado Corradini, Editor-in-Chief, with the assistance of Xunhong Chen, Associate Editor

Keywords:
River restoration
River water level distribution
Groundwater residence time
Groundwater flow and transport modeling
FEFLOW
PEST

SUMMARY

Obtaining a quantitative understanding of river–groundwater interactions is of high practical relevance, for instance within the context of riverbank filtration and river restoration. Modeling interactions between river and groundwater requires knowledge of the river's spatiotemporal water level distribution. The dynamic nature of riverbed morphology in restored river reaches might result in complex river water level distributions, including disconnected river branches, nonlinear longitudinal water level profiles and morphologically induced lateral water level gradients. Recently, two new methods were proposed to accurately and efficiently capture 2D water level distributions of dynamic rivers. In this study, we assessed the predictive capability of these methods with respect to simulated groundwater residence times. Both methods were used to generate surface water level distributions of a 1.2 km long partly restored river reach of the Thur River in northeastern Switzerland. We then assigned these water level distributions as boundary conditions to a 3D steady-state groundwater flow and transport model. When applying either of the new methods, the calibration-constrained groundwater flow field accurately predicted the spatial distribution of groundwater residence times; deviations were within a range of 30% when compared to residence times obtained using a reference method. We further tested the sensitivity of the simulated groundwater residence times to a simplified river water level distribution. The negligence of lateral river water level gradients of 20–30 cm on a length of 200 m caused errors of 40–80% in the calibration-constrained groundwater residence time distribution compared to results that included lateral water level gradients. The additional assumption of a linear water level distribution in longitudinal river direction led to deviations from the complete river water level distribution of up to 50 cm, which caused wide-spread errors in simulated groundwater residence times of 200–500%. For an accurate simulation of groundwater residence times, it is therefore imperative that the longitudinal water level distribution is correctly captured and described. Based on the confirmed predictive capability of the new methods to estimate 2D river water level distributions, we can recommend their application to future studies that model dynamic river–groundwater systems.

1. Introduction

Groundwater flow and transport modeling is a valuable and frequently applied tool to gain a process understanding of surface water–groundwater systems, providing quantitative information on flow paths, mixing ratios and residence times (Wondzell et al., 2009). It is well known from synthetic modeling studies that riverbed morphology affects the river water level distribution, which in turn drives the exchange with groundwater (Cardenas, 2009; Cardenas et al., 2004; Woessner, 2000). Therefore, an important prerequisite for the set up of a groundwater flow and transport model of a real surface water–groundwater system is an accurate description of the water level distribution at the surface water boundary conditions.

A quantitative assessment of groundwater flow paths and residence times is of particular interest for riverbank filtration systems (Tufenkji et al., 2002). Groundwater residence time is an important parameter in determining the effectiveness of the natural attenuation processes that occur during riverbank filtration (Eckert and Irmscher, 2006). River restoration measures, such as riverbed enlargements, potentially lead to reduced groundwater residence times. This, in turn, bears the risk of drinking water contamination (Hoehn and Scholtis, 2011) that contradicts the original purpose of river restoration (Brunke and Gonser, 1997; Woolsey et al., 2007). Groundwater flow and transport modeling could help to mitigate this conflict of interest, by providing a quantitative assessment of

* Corresponding author. Address: Überlandstrasse 133, P.O. Box 611, 8600 Dübendorf, Switzerland. Tel.: +41 58 765 5519; fax: +41 58 765 5028.
E-mail addresses: samuel.diem@eawag.ch (S. Diem), philippe.renard@unine.ch (P. Renard), mario.schirmer@eawag.ch (M. Schirmer).

0022-1694/$ - see front matter © 2014 Elsevier B.V. All rights reserved.
http://dx.doi.org/10.1016/j.jhydrol.2013.12.049

the groundwater flow paths and residence times (Hoehn and Meylan, 2009).

Restored river systems may have complex water level distributions characterized by nonlinear longitudinal water level distributions, morphologically induced lateral water level gradients, disconnected river branches and hydraulic jumps. Such water level distributions need to be characterized by their full spatial (i.e. two horizontal dimensions) and temporal variability and ideally are extracted from hydraulic models (Derx et al., 2010; Doppler et al., 2007; Engeler et al., 2011). However, the setup of a hydraulic model is time consuming and requires a considerable amount of data input. Diem et al. (2013) proposed two new alternative interpolation methods to estimate time-varying one- and two-dimensional (1D, 2D) surface water level distributions of dynamic rivers based directly on measured water level data.

In this study, we assess the predictive capability of the new alternative methods proposed by Diem et al. (2013) with respect to simulated groundwater residence times and the effect of reducing the considered level of detail in the surface water level distribution. Thereto, steady-state surface water level distributions at a partly restored riverbank filtration system are generated with both alternative methods and a reference method, as well as with two simplified methods. The resulting water level distributions are then assigned to a 3D groundwater flow and transport model. After calibration against groundwater heads for each model scenario, the spatial groundwater residence time distribution is predicted within the modeling domain.

2. Interpolation methods

The interpolation methods used in this study are based on those established by Diem et al. (2013). A brief description of the methods is provided in this section, but for a more detailed description the reader is referred to Diem et al. (2013). The new alternative methods and the reference method are referred to as "complete interpolation methods", as they cover the full level of detail including lateral water level gradients and nonlinear longitudinal water level distributions.

2.1. Complete interpolation methods

Both new alternative interpolation methods proposed by Diem et al. (2013) are based on the concept of combining continuous water level records (h^G) from water level gauges (G) with periodic water level measurements (h^F) at fixpoints (F) between water level gauges. By combining this data, the water level distribution between the water level gauges is obtained at a higher resolution. Fixpoints are defined as reference points in the river whose absolute altitude is known. The first alternative "RM method" (Regression of measured data) applies a polynomial regression technique to predict water levels at fixpoints from any water level at a specific water level gauge, while the second alternative "IM method" (Interpolation of measured data) uses a nonlinear interpolation approach between two water level gauges.

Depending on the lateral extent, the river might be considered as a 1D or a 2D domain. In the latter case, the river is discretized by multiple lines parallel to the main flow direction of the river and several sections of support points (S) perpendicular to the flow direction (Fig. 1). Sections of support points are defined at locations where a water level gauge or a fixpoint exists. One fixpoint per section is sufficient to capture the water level distribution across the river unless lateral water level gradients are observed, in which case a fixpoint should be defined on both shorelines.

The water levels at the support points (h^S) are estimated from the water levels at the fixpoint in the simplest possible manner.

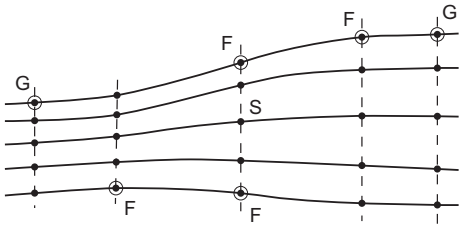

Fig. 1. Schematic illustration of a river system with multiple lines and sections of support points (S, filled black circles). The open black circles indicate the water level gauges (G) and fixpoints (F). Adapted from Diem et al. (2013).

If no lateral water level gradient exists, the water level of the fixpoint is assigned to all support points on the same section. If a second fixpoint was defined to capture lateral gradients, assigning water levels to the support points should be based on field observations. The final interpolation of water levels from the support points to the river boundary nodes of the numerical model is identical for all the interpolation methods and is performed by a linear interpolation along the set of lines.

The third "RH method" (Regression of hydraulic model data) applies a polynomial regression technique, similar to the RM method, but is based on water levels extracted from a hydraulic model at each support point directly. The RH method is therefore considered as reference method among the complete interpolation methods.

2.2. Simplified interpolation methods

In addition to the predictive comparison of the complete interpolation methods described above, we assessed the difference in residence time prediction that evolves when the water level distribution of the river is simplified. Thereto, we applied two progressively simplified methods, both based on the complete IM method. The first simplified method ignores lateral water level gradients and is denoted as "Interpolation of measured data without lateral gradients" (IM_wo_lat). The second simplification additionally assumes a linear interpolation between the river water level gauges and is called "Interpolation of measured data assuming a linear interpolation" (IM_lin).

3. Application to the Niederneunforn field site

This section provides a description of the Niederneunforn field site (Section 3.1) and a review of the implementation of the interpolation methods by Diem et al. (2013) at this field site (Section 3.2). Section 3.3 presents the generated surface water level distributions, which we assigned to the groundwater flow and transport model to simulate the spatial groundwater residence time distribution (see Section 4).

3.1. Field site

The Niederneunforn field site (Fig. 2) is located at the Thur River in NE-Switzerland, approximately 12 km upstream of the confluence with the Rhine River. The Thur River is a peri-alpine river draining a catchment area of 1730 km^2. It is the longest river in Switzerland without a retention basin and therefore has a very dynamic discharge regime. Discharges range from 3 to 1100 m^3/s, with an average discharge of 47 m^3/s.

The field site was instrumented with more than 80 piezometers (2″) during the interdisciplinary RECORD project (Restored corridor dynamics, <http://www.cces.ethz.ch/projects/nature/Record>; Schirmer (2013), Schneider et al. (2011)) in the context of

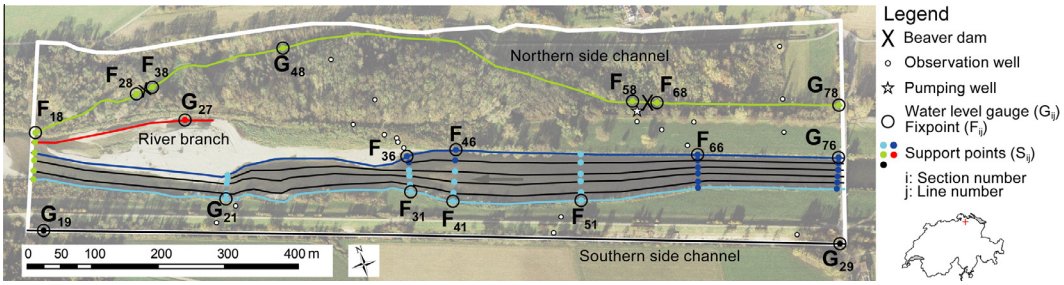

Fig. 2. Niederneunforn field site at the Thur River in NE-Switzerland. Fixpoints and water level gauges in the river and the side channels are shown as open black circles. Based on their position, the set of lines and sections of support points (filled circles) were defined for the implementation of the interpolation methods. The colors of the lines will be used in Fig. 4 again. The colors of the support points in the river indicate the shoreline or the fixpoint/water level gauge on that shoreline from which the water levels were transferred. The general flow direction of the river and the side channels is from right to left. The white polygon represents the modeling domain. Adapted from Diem et al. (2013).

restoration measures that were realized in 2002. The river restoration measures were constrained to the northwestern part of the river reach (Fig. 2). Restoration measures were forbidden in the northeastern part in order to protect the water quality of the nearby pumping station, which supplies the community of Nieder- and Oberneunforn with drinking water. This vertical well produces a total of 36 m^3, split into two daily periods of 1 h and 2 h. At the southern bank of the Thur River, the bank stabilization was maintained to protect the 4 m-high dam, which prevents flooding of nearby farms and agricultural land.

Based on drilling information, the gravel-and-sand aquifer has a thickness of 5.3 ± 1.2 m at the field site. Hydraulic conductivities were estimated to range from 4×10^{-3} to 4×10^{-2} m/s by slug tests, a pumping test and a salt tracer test (Diem et al., 2010; Doetsch et al., 2012). The aquifer is underlain by a lacustrine clay layer, which forms the lower hydraulic boundary. On top of the aquifer is a 0.5–3 m thick layer of silty sand from the alluvial fines that can be regarded as the semi-confining unit. The aquifer varies both spatially and temporally between confined and unconfined. Cross-borehole georadar travel-time tomography revealed an average porosity of 20 ± 3% (Schneider et al., 2011).

At the field site, the width of the Thur River varies between 50 and 100 m (Fig. 2). After the completion of the restoration measures, a large gravel bar has evolved at the downstream end of the river reach. At the same time, a partly disconnected branch of the river developed, which is only flooded at high river stages (>200 m^3/s) and is otherwise fed by groundwater. During low-flow conditions, the river water level profile in the longitudinal direction is nonlinear. In the upstream 400 m, the gradient is 0.5‰ and in the downstream 800 m, it is 2‰. In the central part of the river reach, lateral water level gradients occur during low-flow conditions. These lateral surface water level differences are caused by the asymmetrical riverbed morphology and can reach up to 0.4 m. Two side channels (north and south) flow parallel to the river with widths ranging between 4 and 8 m. Two beaver dams are located in the northern side channel. The upstream dam has a more pronounced effect on water levels, resulting in changes of up to 0.5 m.

3.2. Data collection

Two water level gauges were installed in the main channel of the river, two in each side channel, and one in the river branch (Fig. 2). Several fixpoints were added between the water level gauges to increase the spatial resolution of the water level distribution. In the northern side channel, the fixpoints were placed upstream and downstream of both beaver dams to capture the hydraulic jumps. Fixpoints in the river were placed close to piezometer transects, either on the northern or on the southern shore. In the central portion of the river reach, where lateral water level gradients were observed, a fixpoint was added on either shore. The southern side channel is very straight, has a uniform width, and does not have any obstacles. Therefore, a linear water level distribution was assumed between the water level gauges, which was confirmed by one set of measurements along the channel.

Water levels were measured periodically at the fixpoints between February and May 2011 covering a discharge range of 10–100 m^3/s. The sensors of the water level gauges (DL/N 70, STS AG, Switzerland) have been continuously measuring pressure, temperature and electrical conductivity (EC) at 15-min intervals since April 2010 (error of single measurement: ±0.1% for pressure, ±0.25% for temperature and ±2% for EC, according to the manufacturer's manual). For model calibration, the same type of sensor was placed in each of the observation wells shown in Fig. 2. The raw data of the water level gauges and the observation wells were processed to correct for the barometric air pressure and to transform the pressure data to absolute water levels (m asl).

The system of lines and sections of support points was defined based on the location of water level gauges and fixpoints. Each point can be identified by a uniquely defined indexing system. The first index i refers to the section number and the second index j to the line number (G_{ij}, F_{ij}, S_{ij}). The river was considered to be a 2D domain, described by a set of six lines for the main channel, and one additional line for the disconnected branch. Sections of support points were defined wherever a water level gauge or a fixpoint was located. The colors of the support points in Fig. 2 indicate the shoreline or the fixpoint/water level gauge on that shoreline, from which the water levels were transferred. A lateral gradient of zero was assumed everywhere except for the river sections $i = 3, 4$, where the generally lower water levels of the southern fixpoints were assigned to the support points on lines $j = 1..4$ and the generally higher water levels of the northern fixpoints to the support points on lines $j = 5, 6$ (Fig. 2). Because the width of the northern and southern side channel is much smaller relative to the river width, they were considered as a 1D domain and described by a single line.

For the implementation of the RH method, an existing 2D horizontal hydraulic model of the Thur River was used, which was developed based on the bathymetry measured in September 2009 and covered a discharge range of 10–650 m^3/s (Pasquale et al., 2011; Schäppi et al., 2010). The hydraulic model did not include the side channels and the disconnected river branch. Therefore, the RH method was coupled to the RM method to cover the full surface water level distribution at the Niederneunforn field site.

Fig. 3a shows a 3-month water level time series at the support point S_{46}, determined using the reference RH method (black line). The time series of measured groundwater head at an observation well located 100 m from S_{46} (gray line, Fig. 3a) illustrates the quasi-instantaneous reaction of the groundwater heads to changes in

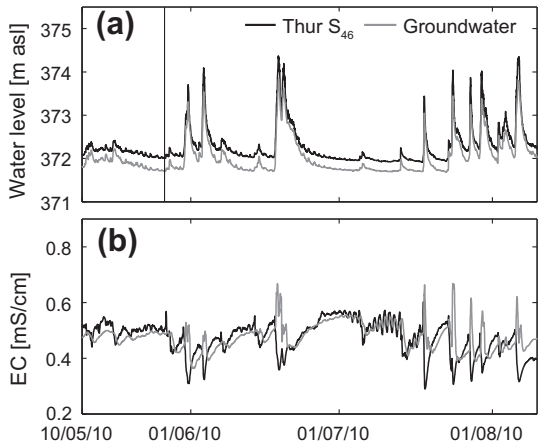

Fig. 3. (a) Water level time series (May to August 2010) generated by the RH method at support point S_{46} in the Thur River (black line) and measured groundwater head time series at a nearby observation well (gray line). The black vertical line indicates the point in time (May 26, 2010, 17:00) for which the surface water level distribution at the field site was generated using each of the five methods (Fig. 4). (b) Time series of electrical conductivity (EC) measurements in the Thur River at the same observation well used in (a).

the river water level, with a propagation speed of about 0.2 m/s or 19600 m/d. Minima in EC, which corresponded with peak flows in the river, were caused by the diluting effect of rain events (Fig. 3b). The characteristic EC signal was identified in all observation wells close to the river, both on its northern and its southern side, which indicates losing conditions. The EC signal in the river was transported into groundwater and was used as a natural tracer. By analyzing the EC time series with nonparametric deconvolution (Cirpka et al., 2007; Vogt et al., 2010), we obtained estimates of local residence time distributions, characterized by a mean (center of gravity) and a standard deviation (Fig. S1 and S2, Table S1; Supporting information). The standard deviation typically amounted to 60–80% of the center of gravity.

In addition to the characteristic EC signal from the river, the groundwater EC signal showed positive spikes, which are presumably caused by mixing of groundwater with higher mineralized pore water during the rise of the groundwater table. These spikes did not affect the residence time distributions determined by nonparametric deconvolution and therefore were not treated in a special manner.

3.3. Generated water level distributions

The surface water level distributions used for the steady-state model simulations were generated with all interpolation methods for the conditions on May 26, 2010 (vertical line in Fig. 3a), which was at the end of a relatively short period of low flow (23 m^3/s). As groundwater heads are highly correlated with the river water levels (Fig. 3a), a steady-state assumption is reasonable.

Fig. 4a shows the spatial water level distributions generated by the three complete interpolation methods. For better clarity, we only plotted the results from one line in the main river channel ($j = 6$, dark blue), which illustrates the nonlinear longitudinal water level distribution. The southern side channel ($j = 9$, black line) had a much lower water level than the river and therefore complied with its purpose of draining groundwater. Water levels in the northern side channel ($j = 8$, green line) were considerably higher because the northern channel flows back to the river at the western end of the field site (river section $i = 1$). The northern side channel could only drain groundwater in one ~400 m segment, where water levels in the side channel were below those in the

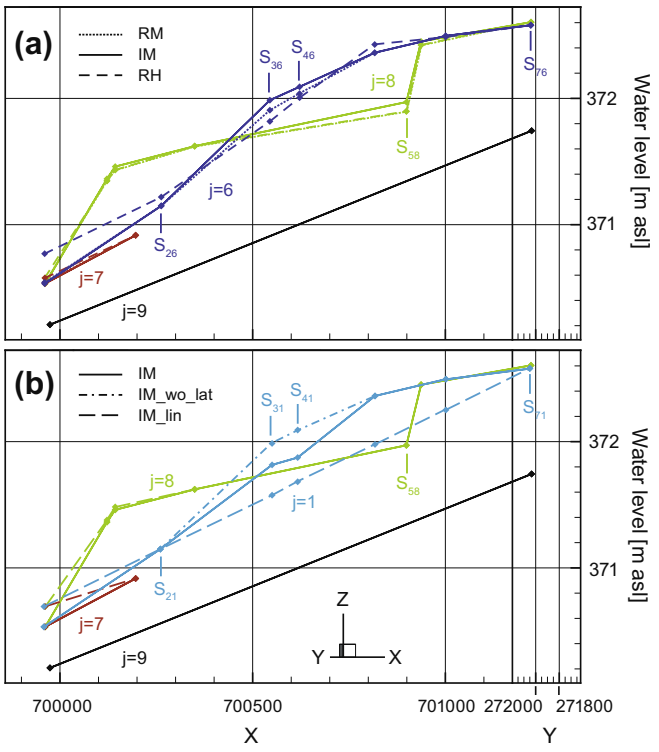

Fig. 4. (a) Spatial water level distribution along the lines $j = 6..9$, generated with the three complete interpolation methods. The figure is orientated for a viewer looking towards NNE, with the flow from right to left. (b) Spatial water level distribution along the lines $j = 1,7..9$, generated with the IM method and its two simplified versions. The water level distributions were generated for the conditions on May 26, 2010, 17:00 (vertical line in Fig. 3a, discharge 23 m^3/s). The colors of the lines correspond to those of Fig. 2 and textures of the lines correspond to the different interpolation methods (see legend).

main river channel. This segment was located downstream of the 50 cm water level drop caused by the eastern beaver dam (S_{58}). The disconnected branch of the river ($j = 7$, red line) showed slightly lower water levels than the main river channel. The disconnected branch and the exfiltrating segment of the northern side channel seemed to be responsible for the river infiltration that occurred to the northern side of the river.

Even though the alternative methods are considered to be accurate in their water level predictions (Diem et al., 2013), single realizations of the spatial water level distribution showed deviations from the reference RH method of mostly 10–20 cm (Fig. 4a). However, errors of more than 30 cm occurred at the river section $i = 1$. As this section was located on a bend in the river, the section did not cross the river perpendicularly. The RH method accounted for the water level gradient across this section by assigning a water level to each of the support points individually, based on the hydraulic model. In contrast, the alternative methods assumed a constant water level across section $i = 1$, as water level information was only available from one fixpoint (F_{18}).

Other deviations in the output from the complete methods were caused by a different data basis (hydraulic model vs. measured data) and/or the different structure of the interpolation methods. The coupling of the RH method to the RM method for the northern and the southern side channel led to identical water level distributions for lines $j = 8, 9$. The IM method showed an identical water level distribution for the southern side channel as well, while deviations from the RM/RH method in the northern side channel reached a maximum of 10 cm at S_{58}.

In Fig. 4b, water level distributions determined from the complete IM method and from the two simplified versions are

depicted. The main river channel is now represented by the southern shoreline ($j = 1$, light blue). The IM method considered lateral water level gradients across sections $i = 3, 4$ where water levels on the southern shoreline $j = 1$ (representative for lines $j = 1..4$, see Fig. 2) were 20–30 cm lower than on the northern shoreline $j = 6$ (representative for lines $j = 5, 6$, see Fig. 2). The first simplified IM method (IM_wo_lat) ignored these lateral water level gradients and the water levels of the northern fixpoints were assigned to all support points on sections $i = 3, 4$. As a consequence, water levels on the southern lines $j = 1..4$ increased by 20 and 30 cm, respectively (Fig. 4b, Fig. 2). The second simplification of the IM method (IM_lin) additionally assumed a linear interpolation between the two water level gauges, which are located at river sections $i = 2, 7$. This assumption caused deviations in water levels of 30–50 cm at the support points in between ($i = 3..6$).

4. Groundwater flow and transport model

4.1. Numerical model set up

We set up a 3D finite-element groundwater flow and transport model using FEFLOW (version 6.0, DHI-WASY GmbH). The modeling domain is shown in Fig. 2. The northern boundary is defined by the northern end of the aquifer and the southern boundary by the southern side channel. The vertical model extent was restricted to the gravel-and-sand aquifer, whose top and bottom elevations were determined from 26 drilling profiles, from which the entire model domain was interpolated by kriging using a linear variogram. The horizontal discretization length of the triangular elements varied between 1 and 5 m around observation wells and along boundaries, including the river and the side channels. In the remaining model domain, the maximal horizontal length of the elements was 10 m. In the vertical direction, the aquifer was subdivided into five layers. The top four layers had a thickness of 1 m and the bottom layer had a variable thickness.

The definition of the boundary conditions is depicted in Fig. 5. We applied an influx boundary condition on the eastern and northern borders (q1 = 0.18 m/d, q2 = 0.0043 m/d), and an outflux boundary condition on the western border (q3 = −0.57 m/d, q4 = −2.3 m/d). These 2nd Type boundary conditions were applied to all layers. We determined the groundwater flux from measured hydraulic gradients and estimated hydraulic conductivities. Recharge was neglected, as no rainfall occurred for ~10 d before the simulation time (Fig. 3a). At the location of the pumping well we assigned an average extraction rate of 36 m^3/d (0.4 L/s).

Within the modeling domain, the southern side channel is exfiltrating along its entire length due to water levels well below those in the river (Fig. 4a). The channel bed sediments are gravelly and tracer tests revealed a good connection to groundwater. We therefore chose a 1D fixed-head boundary condition (1st Type) for the top layer along the southern side channel. For the layers 2–5, a no-flow boundary condition was assigned.

A colmation layer of unknown thickness was identified in the Thur River (Hoehn and Meylan, 2009; Schneider et al., 2011). The bed of the northern side channel consisted of a thick (0.5–1 m) silt and clay colmation layer, except in the middle exfiltrating segment located downstream of the eastern beaver dam, where the bed sediments consisted of sandy gravel. To account for the effect of colmation, we assigned a Cauchy boundary condition (3rd Type) to the river and the northern side channel. In FEFLOW, the colmation layer is characterized by a transfer rate $L = K_r/d_r$. K_r corresponds to the hydraulic conductivity of the colmation layer and d_r to its thickness. The river was described by a 2D Cauchy boundary condition on the top layer, which we subdivided into two zones of transfer rates. Zone L1 (Fig. 5) covered the restored part of the river, including the disconnected branch. The remaining channelized part was covered by zone L2. We split the 1D Cauchy boundary condition along the northern side channel into three zones of transfer rates (L3–L5) to separate the middle exfiltrating segment (L4) (with its gravelly bed sediment) from the upstream and downstream heavily clogged segments.

FEFLOW can describe each transfer rate zone by a transfer rate for infiltration (L_{in}) and exfiltration (L_{out}). In our system, the transfer rate zones L2, L3 and L5 are infiltrating elements and L4 is an exfiltrating element. Only L1 consists of both an infiltrating (main river channel) and an exfiltrating element (disconnected branch). Our system of Cauchy boundary conditions (L1–L5) was therefore characterized by 6 parameters ($L_{in}1$, $L_{in}2$, $L_{in}3$, $L_{in}5$, $L_{out}1$, $L_{out}4$).

L_{out} is typically larger than L_{in}, as the exfiltrating clean groundwater "flushes" the pore space. This effect probably explains the gravelly bed sediments in the southern side channel as well as in the exfiltrating segment of the northern side channel (L4). On the other hand, suspended particles in infiltrating surface water tend to clog the pore space, as it was the case in the main river channel (L1, L2) and in the upstream and downstream part of the northern side channel (L3, L5).

4.2. Calibration procedure

To initially obtain a realistic spatial groundwater residence time distribution when using the reference RH surface water level distribution (Fig. 4a), we jointly estimated the transfer rates and the hydraulic conductivity distribution by fitting both, measured groundwater heads and experimentally determined groundwater residence times from nonparametric deconvolution of EC time series (Section 3.2, Fig. 5). A list of these residence times together with their standard deviations is presented in the Supporting information (Table S1, Fig. S1). To reduce the number of 6 adjustable

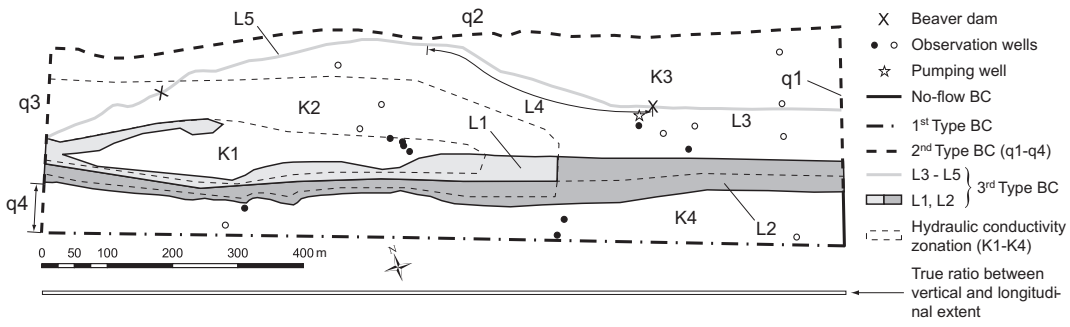

Fig. 5. Spatial definition of the boundary conditions (BCs) and the hydraulic conductivity zonation within the modeling domain. Groundwater head observations were available at all 19 observation wells, while experimentally determined residence times were restricted to 9 observation wells (black filling). The rectangle at the bottom of the figure illustrates the true ratio between the vertical and the longitudinal extent of the model.

Table 1
Hydraulic conductivities and transfer rates of the corresponding parameter zones (Fig. 5) resulting from the initial model calibration using the RH water level distribution. The transfer rates in bold were estimated using PEST. $L_{out}1$ (in brackets) was tied to $L_{in}1$ with a factor of 10. The remaining transfer rates ($L_{in}3$, $L_{in}5$) were kept at their initial values, which in turn were estimated from field observations. The three adjustable transfer rates were estimated for the remaining model scenarios as well (Fig. 6), while the hydraulic conductivity distribution was kept constant.

K1 [m/s]	6×10^{-2}		
K2 [m/s]	2×10^{-2}		
K3 [m/s]	1×10^{-2}		
K4 [m/s]	4×10^{-3}		
$L_{in}1$ [1/d]	**11.9**	$L_{out}1$ [1/d]	**(119)**
$L_{in}2$ [1/d]	**2.1**		
$L_{in}3$ [1/d]	0.5		
		$L_{out}4$ [1/d]	**24.7**
$L_{in}5$ [1/d]	0.5		

transfer rates (Section 4.1), pilot model runs were performed using estimated parameter values from field observations (estimated hydraulic conductivity and approximate thickness of colmation layer). These model runs revealed that the infiltrating main river channel ($L_{in}1$, $L_{in}2$), the exfiltrating disconnected river branch ($L_{out}1$) and the exfiltrating segment of the northern side channel ($L_{out}4$) were responsible for most of the groundwater flux across the Cauchy boundary conditions. $L_{out}1$ was additionally tied to $L_{in}1$ with a factor of 10 to eliminate parameter correlation. For each manual adjustment of the hydraulic conductivity distribution, the remaining three adjustable transfer rates were estimated using PEST (Doherty, 2010) by fitting measured groundwater heads (i.e. minimizing the sum of squared errors between simulated and measured heads). This procedure was iterated until the simulated groundwater residence times (see Section 4.3) were within ±1 standard deviation of the experimentally determined residence times. The resulting hydraulic conductivity distribution comprised four different zones (Fig. 5) and their hydraulic conductivities were within a range of 4×10^{-3}–6×10^{-2} m/s (Table 1), which corresponds well to the measured values (Section 3.1).

Based on this initial parameterization of the reference RH model scenario (Table 1), the water level distributions generated with both alternative and both simplified methods (Fig. 4a and b) were assigned to the river and the side channel boundary conditions of the model. For each of the model scenarios, the three adjustable transfer rates were estimated by fitting measured groundwater heads using PEST to ensure that the basis of the groundwater residence time simulation was a calibration-constrained groundwater flow field. The experimentally determined groundwater residence times were not used as observations for these subsequent model calibrations because groundwater residence time is our key model prediction that will be compared among the different scenarios. Moreover, their exclusion mimics the common situation in practice, where groundwater residence time observations are rarely available. The hydraulic conductivity distribution was not adjusted in the subsequent model calibrations because estimating hydraulic conductivities from groundwater head observations alone was non-unique in our system. Fig. S3 (Supporting information) visually summarizes the initial and the subsequent calibration procedure by a flow chart.

4.3. Simulation of groundwater age

Based on the calibration-constrained groundwater flow field, we simulated the spatial distribution of groundwater residence time, hereafter referred to as groundwater age. According to Goode (1996), the mean groundwater age (i.e. the time since entering the model domain) is obtained by a steady-state transport simulation of a tracer with an appropriate definition of the boundary conditions and a zero-order source term equal to the porosity. A fixed age (concentration) of zero was defined at inflowing boundaries and a natural 2nd Type boundary condition at outflowing boundaries. The latter is described by $n \cdot (D\nabla A) = 0$, i.e. the age (A) in normal direction (n) to the boundary does not change. The zero-order source term was set to 0.2 mg L^{-1} d^{-1} for each element according to the mean porosity of 0.2 (Section 3.1).

We set the longitudinal dispersivity to 10 m for our model on the scale of 1000 m, according to Gelhar et al. (1992). We assigned a value of 1 m to both the horizontal and vertical transverse dispersivity, as differentiating the two was not possible in FEFLOW. As a result, the vertical transverse dispersivity was obviously too high, which caused an excessive vertical dispersion and hence, small vertical age differences. However, as the vertical extent of the modeling domain was very small compared to its horizontal extent (Fig. 5), the groundwater age was mainly controlled by horizontal transport.

To visualize and compare the spatial age distributions from the different model scenarios, we first calculated vertically averaged age distributions, weighted by the element thickness. Additionally, we produced spatial distributions of relative age differences to highlight spatial differences among the age distributions. The relative age difference ΔA_{rel} between a mean age A and a reference mean age A_{ref} was calculated at each node position as follows:

$$\Delta A_{rel} = \frac{A - A_{ref}}{A_{ref}} \cdot 100 \quad (1)$$

5. Results and discussion

5.1. Calibration results

The estimated adjustable transfer rates for all the model scenarios are plotted in Fig. 6. Model scenarios that used the new alternative methods (RM, IM) had small changes in the estimated transfer rates compared to results of the reference RH model scenario (10–40%). Neglecting lateral water level gradients in the first simplified IM method (IM_wo_lat) led to adjustments of the transfer rates by a factor of 2–3 compared to the complete IM method. The largest changes of 1–2 orders of magnitude were made during model calibration of the linear river water level distribution scenario for the second simplified method (IM_lin).

The post-calibration root mean square error (RMSE) between measured and simulated groundwater heads was 7.7 cm for the reference RH method and varied between 7.2 and 7.3 cm for the

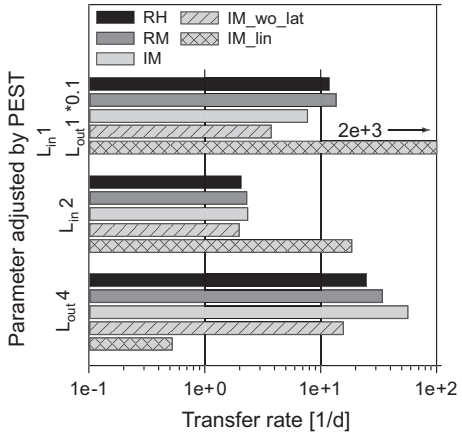

Fig. 6. Post-calibration transfer rates of the reference (RH), the alternative (RM, IM) and the simplified (IM_wo_lat, IM_lin) model scenarios.

RM, the IM as well as for the IM_wo_lat model scenario. The model efficiencies (Mayer and Butler, 1993) were 0.98 for all of the complete methods and the IM_wo_lat method. The IM_lin model scenario resulted in a RMSE of 11 cm and a model efficiency of 0.95. The improvement of the pre-calibration RMSE (using the estimated transfer rates of the RH model scenario; Table 1) over the post-calibration RMSE was small (0.1–0.3 cm) for the alternative methods (RM, IM). For the simplified IM_wo_lat and IM_lin methods, the RMSE was reduced by 2 and 5 cm, respectively.

The inspection of the inversion statistics revealed that the inversion problem was well posed and not infected by a high degree of non-uniqueness. First, the three eigenvalues of the parameter covariance matrix had a maximum to minimum ratio of 10^2, well below the maximum acceptable value of 10^7 (Doherty, 2010). Second, the ratio of the maximum and the minimum composite sensitivity was 9, while the acceptable maximum is 100. The highest correlation of 0.8 was found between $L_{in}2$ and $L_{out}4$. The remaining two correlation coefficients were less than 0.5.

5.2. Groundwater flow field and age distribution

Before being able to compare the age distributions of different model scenarios, we have to become familiar with the general characteristics of the groundwater flow field at our field site. Fig. 7 presents the calibration-constrained groundwater flow field and the corresponding groundwater age distribution from the reference RH model scenario (Fig. 4a). For groundwater recharged by the river or the northern side channel, which was mostly the case within the modeling domain, the groundwater age reflects the "real" age since infiltration. Along the northern and northeastern inflow boundaries (Fig. 5) however, where a fixed age of zero was assigned as well, the groundwater age rather refers to the time since entering the modeling domain.

Infiltration at the main river channel occurred to both the northern and the southern sides, with an overall infiltration rate of 300 L/s. Most of the infiltrated water (about 80%) flowed towards the southern side, due to the high water level gradient between the river and the southern side channel. The corresponding exfiltration rate along the southern side channel (240 L/s) was validated by the measured discharge difference between the water level gauges G_{19} and G_{29} (Fig. 2). Only about 20% of the river infiltration occurred to the northern side, induced by the exfiltrating segment of the northern side channel (L4) and the disconnected branch of the river (Fig. 4a). The model estimated an exfiltration rate of 25 L/s at the exfiltrating segment of the northern side channel, which was consistent with the measured difference in discharge downstream and upstream of the beaver dam. Exfiltration at the disconnected branch occurred at a rate of about 30 L/s.

The groundwater flow field on the southern side of the river was relatively uniform. Infiltration occurred at a steep angle to the river and the groundwater age reached a maximum of 4–8 d. The high water level difference between the river and the southern side channel caused an asymmetric groundwater flow field underneath the river, which significantly contributed to the much higher infiltration towards the southern side.

On the northern side of the river, the flow field was more complex. In the upstream part at river sections $i = 5..7$, infiltration occurred at a relatively steep angle and groundwater flow was directed towards the exfiltrating segment (L4) of the northern side channel. To the north of L4, the low groundwater head gradients and the long flow paths led to groundwater ages of up to 90 d. On the southern side of L4, the groundwater age reached only 10–20 d due to the presence of direct pathways linking the river with the side channel. The pumping well had no significant impact on the groundwater flow field due to its low average pumping rate (Section 4.1).

Further downstream, at river sections $i = 4..5$, the groundwater flow field on the northern side of the river became parallel to the river as the water levels in the northern side channel became higher than those in the main river channel (Fig. 4a). Therefore, groundwater that was not drained by the exfiltrating segment of the northern side channel (L4) was deflected towards and drained by the disconnected branch of the river. The further upstream infiltration at river sections $i = 1..5$ occurred, the longer and the more arc-shaped the flow paths became. Accordingly, the groundwater age increased from the river towards the northern side channel, reaching a maximum of 50 d.

5.3. Predictive comparison of the complete interpolation methods

To assess the predictive capability of both new alternative methods (RM, IM), we calculated the spatial distribution of the relative age difference ΔA_{rel} according to Eq. (1), using the age distribution of the RH method (Fig. 7) as a reference (A_{ref}). Both the RM and the IM model scenario showed similar results (Fig. 8a and b). To the north of the river, two zones with lower ages (10–20%) relative to the RH model scenario were identified between the river sections $i = 2$, 3 and $i = 6$, 7. These small deviations were caused by a combination of minor water level differences with respect to the RH method at river sections $i = 2..5$ (Fig. 4a) and the related changes in transfer rates that occurred during calibration, mostly within 10–40%. These changes actually provided a slightly better fit to the measured groundwater heads (Section 5.1). As an example, the higher water levels of the IM method along river sections $i = 3$, 4 were compensated by a 40% reduction in the $L_{in}1$ transfer rate relative to the RH model scenario (Fig. 6).

The highest adjustment during calibration of the IM model scenario was made for $L_{out}4$, which was doubled to balance the higher water levels in the exfiltrating segment of the northern side channel (Fig. 4a, Fig. 6). A zone of higher groundwater age remained between the river and the northern side channel (Fig. 8b), but deviations were restricted to an upper bound of 30%.

An additional common element of both alternative model scenarios was the zone between the main river channel and the

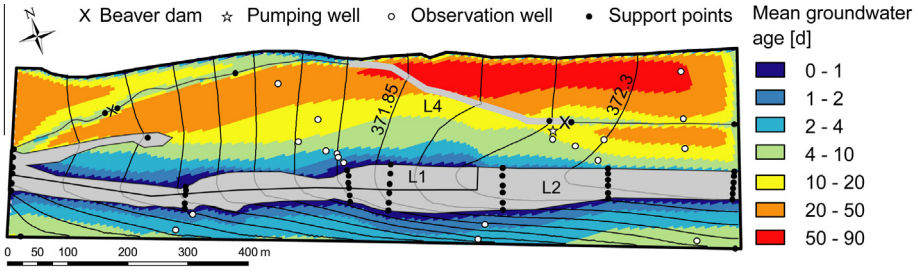

Fig. 7. Calibration-constrained groundwater flow field (shown as groundwater isopotentials with an equidistance of 15 cm) and vertically averaged groundwater age from the reference model scenario using the RH surface water level distribution (Fig. 4a). The three adjustable transfer rate zones are indicated.

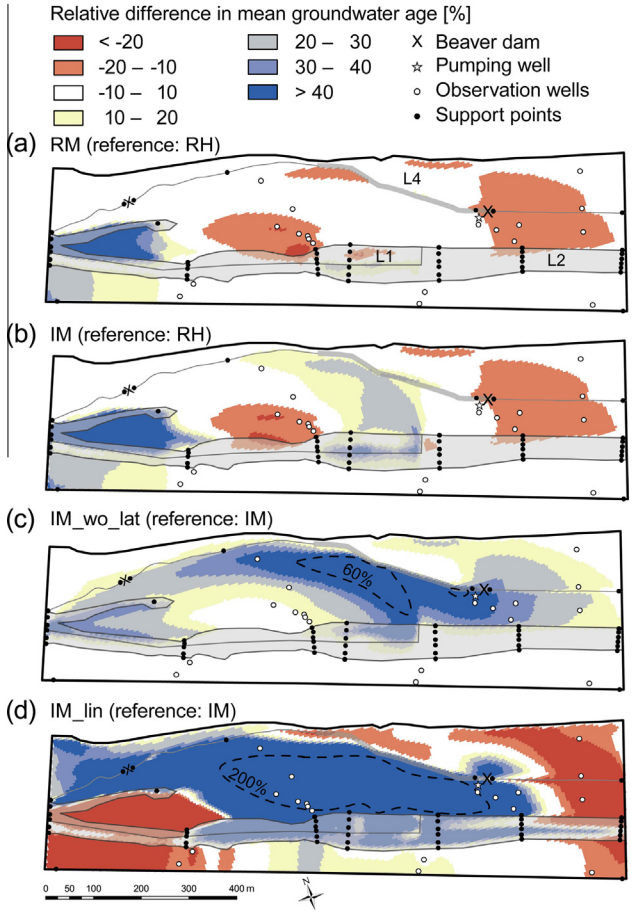

Fig. 8. Spatial distribution of the relative difference in mean groundwater age (Eq. (1)), for the two alternative methods (RM, IM) with respect to the RH method (a and b), and for the two simplified versions of the IM method with respect to the complete IM method (c and d). (c) and (d) contain an additional isoline (black dashed line) of relative age difference of 60% and 200%, respectively. The three adjustable transfer rate zones are indicated.

disconnected branch, where groundwater age differed from the reference model scenario by 40–100%. These deviations can be blamed on the failure of the zero lateral gradient assumption at river section $i = 1$ for both the RM and the IM method (Section 3.3). The too low water levels compared to the RH method could not be compensated for during calibration of the transfer rates as no observations were available in this region, and therefore led to a pronounced increase in groundwater age. Similarly, the underestimation of river water levels at section $i = 1$ of the RM and IM method was also responsible for the positive deviations in groundwater age at the western part of the southern side of the river. Apart from that, errors on the southern side of the river were small (<10%) because river water level deviations were small compared to the difference in water level between the river and the southern side channel.

Besides the large differences between the main river channel and the disconnected branch, both alternative methods (RM, IM) were able to predict the groundwater age within 30% of the reference RH method. The error of 30% is small compared to the uncertainty (standard deviation) of the experimentally determined residence times of 60–80% (Section 3.2). The calibration of the transfer rates compensated for minor differences among the surface water level distributions and the resulting flow fields provided an accurate prediction of groundwater age. These results confirm the capability of the new alternative methods to efficiently capture the relevant characteristics of the surface water level distribution allowing for a reliable simulation of the groundwater age distribution.

5.4. Predictive comparison of the simplified interpolation methods

We used the groundwater age distribution from the IM model scenario as a reference (A_{ref}) to compare the groundwater age distributions of the two simplified model scenarios. Fig. 8c shows the results for the model scenario that applied the first simplified river water level distribution, which ignored lateral water level gradients (IM_wo_lat). The only difference in the water level distribution compared to the full IM implementation was water levels 20–30 cm higher at the support points on river sections $i = 3, 4$ on the southern lines $j = 1..4$ (Fig. 4b, Fig. 2). Even though these changes in the water level distribution seem to be small, the effect on the calibration-constrained groundwater age distribution was considerable. To the north of the river, a band of higher age was identified that extended from the river at sections $i = 4..6$, along the northern side channel, to the disconnected river branch, with deviations of up to 40–80% compared to the IM model scenario.

As described in Section 5.2, the groundwater flow field underneath the river was generally asymmetric because groundwater was largely withdrawn by the strong gradient between the river and the southern side channel. This effect was intensified by the lateral gradient at sections $i = 3, 4$, which was also directed towards the south. Therefore, the negligence of the lateral gradient reduced the asymmetric characteristics and more water infiltrated to the northern side of the river. To counteract this additional groundwater flux and the higher groundwater heads, the $L_{in}1$ transfer rate was lowered by 50% during the calibration procedure (Fig. 6). However, groundwater heads at the upstream observation wells were affected as well, which in turn was compensated by a reduction of the $L_{out}4$ transfer rate by a factor of 3. On the one hand, these adjustments reduced the RMSE to nearly the same level as for the complete IM method (Section 5.1). On the other hand, the direction of the resulting flow field on the northern side of the river was slightly more parallel to the river direction, which caused longer flow paths and longer travel times at the nodes identified by the bluish domain in Fig. 8c.

Fig. 8d depicts the spatial distribution of the relative age difference for the second simplified model scenario that used the IM_lin water level distribution. The assumed linear interpolation between the two water level gauges at river sections $i = 2, 7$ led to lower water levels by up to 50 cm relative to the complete IM implementation (Fig. 4b). Accordingly, the hydraulic gradient between the river and the exfiltrating segment of the northern side channel decreased substantially, which led to a more river-parallel groundwater flow field on the northern side of the river and a widespread increase of 200–500% in groundwater age. In attempt to compensate for the errors in river water levels during calibration against groundwater heads, the $L_{in}1$ and $L_{in}2$ transfer rates were increased by 2 and 1 orders of magnitude, respectively. Additionally, the $L_{out}4$ transfer rate was decreased by 2 orders of magnitude compared to the IM model scenario. Even though the RMSE was reduced from 16 cm to 11 cm, the groundwater flow field and hence the errors in groundwater age prediction could not be improved on the northern side of the river. Instead, the very high $L_{in}1$ transfer rate caused a 20–80% decrease in groundwater age between the river and the disconnected river branch, where the water level differences were similar compared to the complete IM method (Fig. 4b).

The errors in the prediction of groundwater age on the southern side of the river were <10% for the IM_wo_lat model scenario and ranged from −30% in the western part to 30% in the middle part for the IM_lin model scenario. These small changes in groundwater age compared to those on the northern side of the river can be

attributed to the high absolute water level difference between the river and the southern side channel, compared to which the errors in river water levels were small. For instance, the error of 30 cm at the river section $i = 6$ for the simplified IM_lin method reduced the water level gradient between the river and the southern side channel by 30%, compared to the complete IM method (Fig. 4b). In contrast, the same error of 30 cm reduced the water level gradient between the river and the exfiltrating segment of the northern side channel by about a factor of 2.5. This clearly demonstrates that errors in surface water levels have the highest impact on the simulated groundwater age in zones where the water level gradients between infiltrating and exfiltrating boundaries are small.

The description of the river as a 2D domain allowed for including lateral water level gradients. Lateral gradients in river water levels were described in literature, but were explained by stream curvature and the centrifugal force (Cardenas et al., 2004). In restored river reaches, morphologically induced lateral water level gradients are likely to occur quite frequently. At our field site, lateral water level differences of 20–30 cm were restricted to a ~200 m long section (Fig. 4b) and their negligence caused errors in groundwater age prediction of 40–80% (Fig. 8c). When compared to the uncertainty of experimental residence times of 60–80% (Section 3.2), the errors associated with neglecting lateral gradients might be acceptable, depending on the purpose and requirements of the study. At other field sites, however, lateral water level gradients can be more pronounced and their inclusion might be crucial for an accurate groundwater age prediction.

The explicit consideration of the river as a 2D domain was also essential to reliably represent the river's lateral extent and therewith the length of the groundwater flow paths as well as the groundwater residence times. Furthermore, the 2D representation of the river in its full lateral extent allowed us to account for asymmetric groundwater flow underneath the river, which was identified as an important feature influencing the infiltration rates towards the northern and the southern side of the river (Fig. 7, Section 5.2). In previous modeling studies, the river was described as a 2D domain as well, but was cut in approximately the middle where a no-flow boundary condition was assumed (Derx et al., 2010). This assumption suppresses potential asymmetric groundwater flow underneath the river and might lead to a bias in the flow field and the water budget.

Linearly interpolating water levels between water level gauges separated by one or several kilometers is common practice when assigning river water levels to models of river–groundwater systems. Our results revealed that assuming a linear water level distribution can lead to considerable errors in the river water level distribution that translate into inacceptable errors in the simulated groundwater age of >200%. Hence, the accurate description of the longitudinal water level distribution is of major importance for a reliable groundwater age prediction.

6. Conclusions

In this study, we assessed the predictive capability of two new alternative methods for the estimation of 1D and 2D water level distributions of dynamic rivers (RM, IM), with respect to the simulated groundwater residence time (groundwater age). Surface water levels generated with both alternative methods and with a reference method (RH) were assigned to the river and side channel boundary conditions of a 3D groundwater flow and transport model of a partly restored riverbank filtration system in NE-Switzerland. Steady-state model calibration against measured groundwater heads was performed for each of these model scenarios by an automated adjustment of selected transfer rates using PEST. The age predictions of the calibration-constrained groundwater flow fields lay within a range of ±30% compared to the reference RH model scenario. This relatively low error confirmed the predictive capability of the alternative methods when applied to real and complex river-groundwater systems.

We also investigated the sensitivity of the modeled groundwater age distribution to reduced complexity in the river water level distribution. For the first scenario, we modified the IM method to ignore lateral gradients, which led to errors in groundwater age prediction of 40–80% over a considerable area to the north of the river. In the second scenario, we further simplified the IM method by assuming a linear longitudinal water level distribution. As a result, errors in groundwater age of 200–500% were widespread, which demonstrates the importance of an accurate longitudinal water level distribution for the modeled groundwater age.

The results of this study allow us to recommend both alternative approaches presented by Diem et al. (2013) for the river water level assignment in future modeling studies of river–groundwater systems at the kilometer scale. To implement either of the alternative methods at a specific river–groundwater system, the placement of the water level gauges and the fixpoints should be carefully assessed. First, it is important to note that an accurate description of the surface water levels is most important in zones where the gradients between infiltrating and exfiltrating boundaries are small. Second, our results indicate that the longitudinal water level distribution should be captured in detail to reliably simulate the groundwater flow field and the groundwater age distribution. We suggest that, if feasible, water level gauges should be installed at 1 km intervals. In between, fixpoints (e.g. an armor stone or a steel rod) should be installed and leveled with a spacing that is inversely proportional to the change in surface water level gradient and might range from 50 to 200 m. For instance, a segment with a linear water level profile can be captured by two fixpoints, while a segment with a changing gradient requires three or more fixpoints. Additionally, fixpoints should be installed upstream and downstream of a hydraulic jump, for example at beaver dams or weirs. To maximize the accuracy in groundwater age prediction, we recommend the inclusion of lateral water level gradients by defining two fixpoints on the same section.

This study demonstrates that a reduced level of detail in the river water level distribution can lead to considerable errors in simulated groundwater flow paths and residence times. Therefore, it is essential to capture the river water level distribution in its full spatial and temporal extent. To this end, the new methods proposed by Diem et al. (2013) proved to offer an accurate and efficient alternative compared to using a hydraulic model. The application of these interpolation methods when modeling riverbank filtration systems will, for instance, help to reliably assess the impact of river restoration measures on groundwater residence times and hence, to mitigate the conflict of interest between river restoration and drinking water protection.

Acknowledgments

This study was conducted within the National Research Program "Sustainable Water Management" (NRP61) and funded by the Swiss National Science Foundation (SNF, Project No. 406140-125856). We would like to thank Matthias Rudolf von Rohr, Lena Froyland and Urs von Gunten for their support. We warmly thank Ryan North and John Molson for many helpful discussions. The Agency for Environment of the Canton Thurgau provided data, logistics and financial support. Additional support was provided by the Competence Center Environment and Sustainability (CCES) of the ETH domain in the framework of the RECORD (Assessment and Modeling of Coupled Ecological and Hydrological Dynamics in the Restored Corridor of a River (Restored Corridor Dynamics)) and RECORD Catchment projects.

Appendix A. Supplementary material

Supplementary data associated with this article can be found, in the online version, at http://dx.doi.org/10.1016/j.jhydrol.2013.12.049.

References

Brunke, M., Gonser, T., 1997. The ecological significance of exchange processes between rivers and groundwater. Freshwater Biol. 37 (1), 1–33.

Cardenas, M.B., 2009. Stream–aquifer interactions and hyporheic exchange in gaining and losing sinuous streams. Water Resour. Res. 45, 1–13.

Cardenas, M.B., Wilson, J.L., Zlotnik, V.A., 2004. Impact of heterogeneity, bed forms, and stream curvature on subchannel hyporheic exchange. Water Resour. Res. 40 (8), 1–13.

Cirpka, O.A., Fienen, M.N., Hofer, M., Hoehn, E., Tessarini, A., Kipfer, R., Kitanidis, P.K., 2007. Analyzing bank filtration by deconvoluting time series of electric conductivity. Ground Water 45 (3), 318–328.

Derx, J., Blaschke, A.P., Blöschl, G., 2010. Three-dimensional flow patterns at the river-aquifer interface – a case study at the Danube. Adv. Water Resour. 33 (11), 1375–1387.

Diem, S., Vogt, T., Hoehn, E., 2010. Spatial characterization of hydraulic conductivity in alluvial gravel-and-sand aquifers: a comparison of methods. Grundwasser 15 (4), 241–251.

Diem, S., Renard, P., Schirmer, M., 2013. New methods to estimate 2D water level distributions of dynamic rivers. Ground Water 51 (6), 847–854.

Doetsch, J., Linde, N., Vogt, T., Binley, A., Green, A.G., 2012. Imaging and quantifying salt-tracer transport in a riparian groundwater system by means of 3D ERT monitoring. Geophysics 77 (5), B207–B218.

Doherty, J., 2010. Model-independent Parameter Estimation. User Manual, fifth ed. Watermark Numerical Computing, Brisbane, pp. 336.

Doppler, T., Hendricks Franssen, H.J., Kaiser, H.P., Kuhlman, U., Stauffer, F., 2007. Field evidence of a dynamic leakage coefficient for modelling river–aquifer interactions. J. Hydrol. 347 (1–2), 177–187.

Eckert, P., Irmscher, R., 2006. Over 130 years of experience with riverbank filtration in Düsseldorf. Germany. J. Water Supply Res. T. 55 (4), 283–291.

Engeler, I., Hendricks Franssen, H.J., Müller, R., Stauffer, F., 2011. The importance of coupled modelling of variably saturated groundwater flow-heat transport for assessing river-aquifer interactions. J. Hydrol. 397 (3–4), 295–305.

Gelhar, L.W., Welty, C., Rehfeldt, K.R., 1992. A critical review of data on field-scale dispersion in aquifers. Water Resour. Res. 28 (7), 1955–1974.

Goode, D.J., 1996. Direct simulation of groundwater age. Water Resour. Res. 32 (2), 289–296.

Hoehn, E., Meylan, B., 2009. Measures to protect drinking-water wells near rivers from hydraulic engineering operations in peri-alpine flood-plains. Grundwasser 14 (4), 255–263.

Hoehn, E., Scholtis, A., 2011. Exchange between a river and groundwater, assessed with hydrochemical data. Hydrol. Earth Syst. Sci. 15 (3), 983–988.

Mayer, D.G., Butler, D.G., 1993. Statistical validation. Ecol. Model. 68 (1–2), 21–32.

Pasquale, N., Perona, P., Schneider, P., Shrestha, J., Wombacher, A., Burlando, P., 2011. Modern comprehensive approach to monitor the morphodynamic evolution of a restored river corridor. Hydrol. Earth Syst. Sci. 15 (4), 1197–1212.

Schäppi, B., Perona, P., Schneider, P., Burlando, P., 2010. Integrating river cross section measurements with digital terrain models for improved flow modelling applications. Comput. Geosci. 36 (6), 707–716.

Schirmer, M., 2013. Das RECORD-Projekt - Flussrevitalisierung, eine ökologische Massnahme in einem komplexen Umfeld. Aqua und Gas 3, 22–28.

Schneider, P., Vogt, T., Schirmer, M., Doetsch, J., Linde, N., Pasquale, N., Perona, P., Cirpka, O.A., 2011. Towards improved instrumentation for assessing river–groundwater interactions in a restored river corridor. Hydrol. Earth Syst. Sci. 15 (8), 2531–2549.

Tufenkji, N., Ryan, J.N., Elimelech, M., 2002. The promise of bank filtration. Environ. Sci. Technol. 36 (21), 422A–428A.

Vogt, T., Hoehn, E., Schneider, P., Freund, A., Schirmer, M., Cirpka, O.A., 2010. Fluctuations of electrical conductivity as a natural tracer for bank filtration in a losing stream. Adv. Water Resour. 33 (11), 1296–1308.

Woessner, W.W., 2000. Stream and fluvial plain ground water interactions: rescaling hydrogeologic thought. Ground Water 38 (3), 423–429.

Wondzell, S.M., LaNier, J., Haggerty, R., 2009. Evaluation of alternative groundwater flow models for simulating hyporheic exchange in a small mountain stream. J. Hydrol. 364 (1–2), 142–151.

Woolsey, S., Capelli, F., Gonser, T., Hoehn, E., Hostmann, M., Junker, B., Paetzold, A., Roulier, C., Schweizer, S., Tiegs, S.D., Tockner, K., Weber, C., Peter, A., 2007. A strategy to assess river restoration success. Freshwater Biol. 52 (4), 752–769.